Research Article

Knockout of the Tumor Suppressor Gene *Gprc5a* in Mice Leads to NF-κB Activation in Airway Epithelium and Promotes Lung Inflammation and Tumorigenesis

Jiong Deng[1], Junya Fujimoto[1], Xiao-Feng Ye[1], Tao-Yan Men[1], Carolyn S. Van Pelt[2], Yu-Long Chen[1], Xiao-Feng Lin[1], Humam Kadara[1], Qingguo Tao[1], Dafna Lotan[1], and Reuben Lotan[1]

Abstract

Mouse models can be useful for increasing the understanding of lung tumorigenesis and assessing the potential of chemopreventive agents. We explored the role of inflammation in lung tumor development in mice with knockout of the tumor suppressor *Gprc5a*. Examination of normal lung tissue and tumors from 51 *Gprc5a*$^{+/+}$ (adenoma incidence, 9.8%; adenocarcinoma, 0%) and 38 *Gprc5a*$^{-/-}$ mice (adenoma, 63%; adenocarcinoma, 21%) revealed macrophage infiltration into lungs of 45% of the *Gprc5a*$^{-/-}$ mice and 8% of *Gprc5a*$^{+/+}$ mice and the direct association of macrophages with 42% of adenomas and 88% of adenocarcinomas in the knockout mice. *Gprc5a*$^{-/-}$ mouse lungs contained higher constitutive levels of proinflammatory cytokines and chemokines and were more sensitive than lungs of *Gprc5a*$^{+/+}$ mice to stimulation of NF-κB activation by lipopolysaccharide *in vivo*. Studies with epithelial cells cultured from tracheas of *Gprc5a*$^{-/-}$ and *Gprc5a*$^{+/+}$ mice revealed that *Gprc5a* loss is associated with increased cell proliferation, resistance to cell death in suspension, and increased basal, tumor necrosis factor α–induced, and lipopolysaccharide-induced NF-κB activation, which were reversed partially in *Gprc5a*$^{-/-}$ adenocarcinoma cells by reexpression of *Gprc5a*. Compared with *Gprc5a*$^{+/+}$ cells, the *Gprc5a*$^{-/-}$ cells produced higher levels of chemokines and cytokines and their conditioned medium induced more extensive macrophage migration. Silencing *Gprc5a* and the p65 subunit of NF-κB in *Gprc5a*$^{+/+}$ and *Gprc5a*$^{-/-}$ cells, respectively, reversed these effects. Thus, *Gprc5a* loss enhances NF-κB activation in lung epithelial cells, leading to increased autocrine and paracrine interactions, cell autonomy, and enhanced inflammation, which may synergize in the creation of a tumor-promoting microenvironment. *Cancer Prev Res; 3(4); 424–37. ©2010 AACR.*

Introduction

Lung cancer, the leading cause of cancer-related deaths, is linked mainly to tobacco smoking (1). However, host factors, both genetic and epigenetic, also play important roles in lung carcinogenesis. For example, pulmonary inflammation has been implicated in the development of lung cancer in humans (2) and in mouse models (3, 4). Besides causing DNA damage and mutations, tobacco smoke also induces chronic pulmonary inflammation, which can promote carcinogenesis (5), especially in cases where it also leads to chronic obstructive pulmonary disease (6, 7). Furthermore, the development of lung cancers is strongly correlated with pulmonary inflammation even in nonsmokers (8). Interestingly, anti-inflammatory drugs can reduce lung tumorigenesis in mouse models (2, 4, 9, 10) and incidence of lung cancer, especially adenocarcinomas, in humans (11). Inflammatory cells, especially tumor-associated macrophages and neutrophils, play important roles in conditioning the microenvironment by releasing numerous inflammatory cytokines, chemokines, and growth factors that can act on epithelial cells and enhance transformation and progression into premalignant, malignant, and metastatic lesions (12, 13). Therefore, targeting inflammation is considered to be a promising approach to chemoprevention and treatment of lung cancer (14, 15).

Many effects of chronic inflammation are mediated by NF-κB, a transcription factor that controls the expression of genes involved in inflammation, immune responses, cell cycle, apoptosis, and angiogenesis in a variety of cells, including epithelial cells, stromal cells, and macrophages (16, 17). Thus, NF-κB activation and signaling pathway link inflammation and cancer.

Authors' Affiliations: Departments of [1]Thoracic/Head and Neck Medical Oncology and [2]Veterinary Medicine and Surgery, The University of Texas M.D. Anderson Cancer Center, Houston, Texas

Note: J. Deng and J. Fujimoto contributed equally to this work and should be considered first authors.

Current address for J. Deng: Key Laboratory of Cell Differentiation and Apoptosis, Department of Pathophysiology, Shanghai Jiao-Tong University School of Medicine, Shanghai 200025, China.

Corresponding Author: Reuben Lotan, Department of Thoracic/Head and Neck Medical Oncology, The University of Texas M.D. Anderson Cancer Center, Houston, TX 77030. Phone: 713-792-8467; Fax: 713-745-5656; E-mail: rlotan@mdanderson.org.

American Association for Cancer Research

Recently, we have shown that deletion of a retinoic acid–inducible orphan G protein–coupled receptor, *Gprc5a* (18, 19), which is expressed preferentially in lung tissue, predisposes mice to develop spontaneous lung tumors, indicating that it functions as a lung-specific tumor suppressor (20). The carcinogenesis process in the *Gprc5a* knockout (*Gprc5a*$^{-/-}$) mouse takes 1 to 2 years, emulating the long latency typical for human lung cancer development (20). However, the events that presumably take place during this period in the *Gprc5a* knockout mice are not understood.

Here, we report that the loss of *Gprc5a* in mouse lung epithelial cells results in activation of NF-κB and expression of various cytokines and chemokines *in vitro* and *in vivo*. These factors increase the proliferation and survival of the epithelial cells as well as induce infiltration of macrophages into the mouse lungs, leading to the development of acidophilic macrophage pneumonia (AMP; ref. 21) and the ensuing inflammation. We propose that the increased epithelial cell proliferation and resistance to cell death and the development of an inflammatory microenvironment in the lungs of *Gprc5a* knockout mice act in concert to promote tumorigenesis.

Materials and Methods

Animals

We used (129sv × C57BL/6) F1 *Gprc5a* wild-type and *Gprc5a* knockout mice, which recently have been named *Gprc5a*^{tm1Rlo}/*Gprc5a*^{tm1Rlo} (Gprc5a, G protein–coupled receptor, family c, group 5, member A; tm1, targeted mutation 1; Rlo, Reuben Lotan) by the Mouse Genome Informatics, The Jackson Laboratory. In the current study, the wild-type and knockout mice are called *Gprc5a*$^{+/+}$ and *Gprc5a*$^{-/-}$ mice, respectively. The mice were generated and maintained according to a protocol approved by the M.D. Anderson Institutional Animal Care and Use Committee as described (20).

Analysis of mouse lungs for identification of tumors, macrophages, and microvessels by histology and immunohistochemistry

Mouse lungs were excised, fixed in formalin, and embedded in paraffin. Sections (5 μm thick) of lung tissue and tumor specimens were stained with H&E and observed under the microscope by a veterinary pathologist (C.S.V.P) for diagnosis of adenoma, adenocarcinoma, and AMP according to histologic criteria described previously (21–23). The AMP was graded as follows: grade 1 (5-10% macrophages in a microscopic field), grade 2 (10-20%), grade 3 (20-50%), and grade 4 (>50%). Macrophages were also identified by subjecting lung tissue sections to an antigen retrieval procedure using proteinase K (DAKO) before incubation with rat antibodies against mouse F4/80 (AbD Serotec). Subsequently, the sections were incubated with goat anti-rat secondary antibody (Vector) followed by incubation with avidin-biotin-peroxidase complex (DAKO) and development with diaminobenzidine chromogen (DAKO) and counterstaining with hematoxylin. Immunohistochemical analyses of the staining reactivity were done in duplicate on inflammation areas and tumors. Microvessel density (MVD) was determined by staining tissue sections with antibodies against the CD31 antigen (BD Pharmingen) using a similar procedure as described above. The staining intensities for each antigen were quantified by counting the number of cells exhibiting positive reactivity in two separate microscopic fields.

Analysis of cytokines and chemokines

Lungs from *Gprc5a*$^{+/+}$ and *Gprc5a*$^{-/-}$ mice (*n* = 5; 4 mo old) were excised, homogenized, and extracted for analysis by Proteome Profiler Mouse Cytokine Array, Panel A, which includes immobilized antibodies against 40 cytokines and chemokines (R&D Systems) using the manufacturer's instructions.

Treatment of mice with lipopolysaccharide

Five-month-old *Gprc5a*$^{+/+}$ and *Gprc5a*$^{-/-}$ mice were injected i.p. with 0.2 mL of a solution of 50 μg/mL lipopolysaccharide (LPS) in PBS (*Escherichia coli* strain O111:B4; Sigma Chemical Co.) or 0.2 mL PBS (control) and killed 4 h later. Their lungs were excised and processed for (*a*) analysis of tumor necrosis factor α (TNFα) levels by Quantikine Immunoassay (R&D Systems), (*b*) Western blot analysis of Ym1 protein, (*c*) preparation of nuclear extract for NF-κB DNA-binding analysis by electrophoretic mobility shift assay (EMSA), and (*d*) fixation in formalin for immunohistochemical analysis of tissue sections for localization of the NF-κB subunit p65 as described below.

Immunoblotting

The procedure was done as described previously (24). Primary polyclonal rabbit antibodies against the following antigens were purchased from the following sources: Ym1 from StemCell Technologies, IκBα (C-21) and p65 (A) from Santa Cruz Biotechnology, and actin from Sigma-Aldrich. Rabbit antibodies against the mouse Gprc5a COOH-terminal peptide were described (20). Mouse monoclonal antibodies against a Myc epitope peptide tag were from Upstate Biotechnology.

Detection of NF-κB by immunohistochemistry

Histologic sections of formalin-fixed and paraffin-embedded lung tissue were incubated with Target Retrieval Solution (pH 6.0; DAKO) and then subjected to sequential incubations with rabbit polyclonal antibody against NF-κB p65 (eBioscience), peroxidase-conjugated anti-rabbit antibody (EnVision$^+$ Systems, DAKO), and 3,3′-diaminobenzidine.

Electrophoretic mobility shift assay

NF-κB DNA-binding activity in nuclear extracts prepared from lung tissues or cell lines (see below) was examined as described (24). The following oligonucleotides were used for the analysis: wild-type NF-κB–binding oligonucleotide,

5′-CGGAAAGTCCCCAGCGGAAAGTCCCTGAT-3′; mutant NF-κB–binding oligonucleotide, 5′-CGGAAAGTgag-CAGCGGAAAGTGagTGAT-3′.

Isolation, characterization, and maintenance of mouse tracheal epithelial cells and mouse lung adenocarcinoma cells

Epithelial cells were isolated in our laboratory from tracheas dissected from 3-wk-old $Gprc5a^{+/+}$ and $Gprc5a^{-/-}$ mice. The tracheas were minced into 1-mm^3 pieces, which were incubated in a tissue-dissociating solution ACCU-MAX (Innovative Cell Technologies). The dissociated cells and tissue fragments were then transferred to PRIMARIA tissue culture dishes (BD Biosciences) and incubated in AmnioMAX-C100 medium (Invitrogen), which facilitated epithelial cell growth. The epithelial cells that have grown in these dishes were detached by trypsin treatment and then subcultured and grown in keratinocyte serum-free medium (Life Technologies; Invitrogen), and aliquots were frozen in liquid nitrogen. The epithelial cells were designated $Gprc5a^{+/+}$ and $Gprc5a^{-/-}$, respectively. The cells were karyotyped by G banding in the M.D. Anderson Institutional Molecular Cytogenetics Facility and found to be of mouse origin. For analysis of mutations in Trp53 and Kras, DNA was purified from the cells using reagents from Qiagen, Inc. The analysis was done by Genewiz, Inc. PCR primers designed by the company were used to amplify exons 1 and 2 of the mouse Kras gene and exons 5, 6, 7, and 8 of the mouse Trp53 for sequence comparisons between $Gprc5a^{-/-}$ and $Gprc5a^{+/+}$ cells. Twenty-five nanograms of genomic DNA were suspended in 25 µL of PCR buffer containing 25 mmol/L MgCl$_2$, 5 µmol/L specific primer pairs, 10 mmol/L deoxynucleotide triphosphates, and 0.5 µL Taq polymerase (HotStar Taq, Qiagen). DNA was sequenced using an Applied Biosystems 3730xl DNA Sequencer. The same primers used for PCR amplification were also used for sequencing. The mouse lung cell line 959(−/−) was derived from an adenocarcinoma tumor in the lung of a 2-y-old $Gprc5a^{-/-}$ male mouse using methods described before (20).

Cell proliferation assay

Cells were seeded in replicate wells of 96-well plates and grown for 1 to 5 d. The final cell number was estimated using the MTT viability assay.

mRNA analysis and real-time PCR

RNA extracted from lung epithelial cells using Tri-Reagent (Molecular Research Center) was reverse transcribed into cDNA by RETROscript First Strand Synthesis kit (Ambion). The cDNAs were subjected to quantitative PCR using primers for quantitative PCR and Taqman Gene Expression Master Mix from Applied Biosystems. Mouse actin was used as an internal control gene. The expression data were analyzed and normalized to actin using the 7500 Fast System Software from Applied Biosystems. For duplex reverse transcription-PCR (RT-PCR), cDNA was amplified with the $Gprc5a$ primers (20) plus β-actin competition primers from Ambion in High-Fidelity PCR Master Mix (Roche).

Cell survival in suspension and fluorescence-activated cell sorting analyses

Lung epithelial cells were suspended in keratinocyte serum-free medium and dispensed into six-well plates coated with the nonadhesive polymer poly(2-hydroxyethylmethacrylate) (PolyHEMA; Sigma-Aldrich) to prevent cell attachment and induce anoikis (25). After 24 or 48 h, cells were harvested, fixed, stained with propidium iodide, and subjected to fluorescence-activated cell sorter analysis (Coulter EPICS Profile II Flow Cytometer). The sub-G$_1$ cell population was considered to represent dead cells.

Immunofluorescent staining for p65 localization

Lung epithelial cells were cultured on glass coverslips, fixed with formaldehyde, permeabilized, and incubated with monoclonal antibody to p65 (eBioscience) followed by FITC-conjugated secondary antibody (Molecular Probes). Cells were analyzed using a fluorescence microscope, and digital images of FITC staining were captured.

Macrophage migration analysis

For these studies, we used the mouse alveolar macrophage-like cell line MH-S, a continuously proliferating cell line of SV40-transformed alveolar macrophages isolated by bronchoalveolar lavage from BALB/c mice (26). These cells have been chosen because they express many phenotypic and functional characteristics of freshly isolated alveolar macrophages (26, 27) and have been used previously to assess macrophage migration (28).

The cells were propagated in RPMI 1640 with 10% fetal bovine serum but were starved for 24 h in serum-free RPMI 1640 before the migration assay. For the assay, 6,000 cells suspended in 150 µL of serum-free RPMI 1640 were placed in the upper insert of a Boyden chamber (BD Falcon), which has at its bottom a polyethylene terephthalate membrane with 8-µm pores (Becton Dickinson), and the inserts were placed inside wells of a 24-well plate (BD Falcon) containing serum-free conditioned medium isolated from 48-h cultures of mouse $Gprc5a^{+/+}$ and $Gprc5a^{-/-}$ lung epithelial cells. Twenty-four or 48 h later, the inserts were fixed in 90% ethanol and the MH-S cells remaining in the upper surface of the membrane were removed using a cotton tip swab and cells that had migrated to the underside of the membrane were stained with 1% crystal violet, and the membrane was observed under the microscope for detection, counting, and photography of migrated cells.

In exploratory experiments, we found that the migration of the MH-S cells after 24-h incubation with conditioned medium from $Gprc5a^{-/-}$ lung epithelial cells was low (<40 cells per microscopic field) but the number of migrating cells increased to ~400 cells per field after 48 h. After determining that the serum-free conditioned medium of either $Gprc5a^{+/+}$ or $Gprc5a^{-/-}$ cells did not enhance the growth

of the MH-S cells during a 48-h migration assay, we did all migration experiments for 48 h.

Silencing genes by transfection of cells with small interfering RNAs

Small interfering RNAs (siRNA) against p65 (Rel A mouse ON-TargetPlus SMARTpool), against *Gprc5a*, or nonspecific siRNA was from Dharmacon. Transfection was done using X-tremeGENE siRNA transfection reagent (Roche). The medium was then harvested and centrifuged, and the supernatant was used for macrophage migration assay. Some replicate plates were used for harvesting and processing cells for immunoblotting, EMSA, and/or RT-PCR analysis of selected cytokines and chemokines.

Differential expression of NF-κB target genes

We used data on global gene expression obtained previously by Affymetrix GeneChip Mouse Genome 430 2.0 array analysis of RNA isolated from *Gprc5a*$^{+/+}$ and *Gprc5a*$^{-/-}$ epithelial cells.[3] The differential expression of genes reported to be targets of NF-κB (http://bioinfo.lifl.fr/NF-KB/) was derived from the microarray data based on the *P* value of a random variance two-sample *t* test with permutation with estimation of the false discovery rate and a fold difference in expression. Only genes with *Gprc5a*$^{-/-}$/*Gprc5a*$^{+/+}$ fold change of >2 were selected for presentation.

Statistical analysis

Differences in tumor incidence and inflammation between *Gprc5a*$^{+/+}$ and *Gprc5a*$^{-/-}$ were analyzed for statistical significance by a two-sided Fisher's exact test using the R 2.6.0 statistical package (http://www.r-project.org). Differences between expression of the macrophage marker F4/80 and the endothelial cell marker CD31 in adenomas and adenocarcinomas as well as expression of chemokine and cytokine in *Gprc5a*$^{+/+}$ and *Gprc5a*$^{-/-}$ cells with or without transfection of siRNA or *Gprc5a* and induction of macrophage migration by conditioned medium were analyzed for statistical significance using the two-tailed Student's *t* test. *P* values of <0.05 were considered to be statistically significant.

Results

Increased macrophage infiltration into lungs of *Gprc5a*$^{-/-}$ mice compared with *Gprc5a*$^{+/+}$ mice and its association with tumor incidence

Observation of H&E-stained histologic sections of lung specimens from *Gprc5a*$^{+/+}$ (wild-type) mice and *Gprc5a*$^{-/-}$ (knockout) mice collected in our previous study (20) revealed the presence of AMP associated with lung tumors (both adenoma and adenocarcinomas; Fig. 1A). To relate the presence of inflammatory cells to tumor development, we examined their incidence and association. Figure 1B shows that 24 of 38 of the *Gprc5a*$^{-/-}$ mice developed ade-

nomas and 8 of 38 developed adenocarcinomas, whereas only 5 of 51 wild-type mice developed adenomas and none (0 of 51) developed an adenocarcinoma (*P* = 10^{-6} and 0.0007, respectively, when compared with *Gprc5a*$^{-/-}$ mice). The incidence of AMP was significantly (*P* = 0.003) higher in the *Gprc5a*$^{-/-}$ (17 of 38, 45%) than in the *Gprc5a*$^{+/+}$ mouse lungs (4 of 51, 7.8%; Fig. 1B). Notably, in the *Gprc5a*$^{-/-}$ mice, AMP was associated with 10 of 24 (41.6%) adenomas and with 7 of 8 (87.5%) adenocarcinomas (Fig. 1B, right), whereas none of the adenomas in the *Gprc5a*$^{+/+}$ mice was associated with AMP (Fig. 1B, left).

In the *Gprc5a*$^{+/+}$ mice, 6 of 51 had lymphoid proliferation compared with 2 of 38 in the knockout mice, and there was no relationship between lymphoid proliferation and tumor development. Immunohistochemical analysis of sections of one lymphoid nodule that was available from a *Gprc5a*$^{-/-}$ mouse lung revealed that most of the lymphocytes (>80%) were positive for CD45R (commonly expressed on all B and subset of memory T lymphocytes) and 5% to 10% were positive for CD4 (expressed on T cells that bind epitopes in class I histocompatibility molecules) and CD8 (expressed on T cells that bind epitopes in class II histocompatibility molecules; data not shown).

Further immunohistochemical analysis of specimens from *Gprc5a*$^{-/-}$ mice including 10 adenomas (from 10 mice) and 8 adenocarcinomas (from 7 mice) using antibodies against F4/80, a marker of mature tissue macrophages (29), revealed that all those specimens had large numbers of F4/80$^+$ cells located in the periphery of tumors and fewer macrophages that had infiltrated into the center of the lesions (Fig. 1C, four panels on bottom left). There was no statistically significant difference between adenomas and adenocarcinomas in the prevalence of F4/80$^+$ cells in the periphery or within the tumors (Fig. 1C, bar graphs on bottom right).

Because inflammation can affect angiogenesis, we compared MVD by quantitation of CD31$^+$ cells in histologic sections of lung tumors. No statistically significant differences in MVD were found between six adenomas and six adenocarcinomas (mean ± SD: 26.08 ± 5.08 and 30.71 ± 4.83 vessels per microscopic field, respectively) or between six tumors with no or low-grade AMP (0 and 1) and six tumors with higher-grade AMP (3 and 4; 30.50 ± 8.61 and 26.29 ± 5.70 vessels per microscopic field, respectively). However, MVD in four cases with the most severe AMP (grade 4) was significantly lower than in eight cases with lower-grade AMP (<3; 18.50 ± 3.58 and 33.34 ± 3.77 vessels per field, respectively; *P* = 0.032, unpaired *t* test).

An increased inflammatory status in *Gprc5a*$^{-/-}$ mouse lungs

To begin to understand the mechanism underlying the preferential infiltration of macrophages into *Gprc5a*$^{-/-}$ mouse lungs, we compared the levels of 40 proinflammatory chemokines and cytokines in normal lung tissues of 5-month-old *Gprc5a*$^{-/-}$ and *Gprc5a*$^{+/+}$ mice. This age has been chosen because it precedes the appearance of tumors by 6 to 7 months. The levels of 23 cytokines and

---

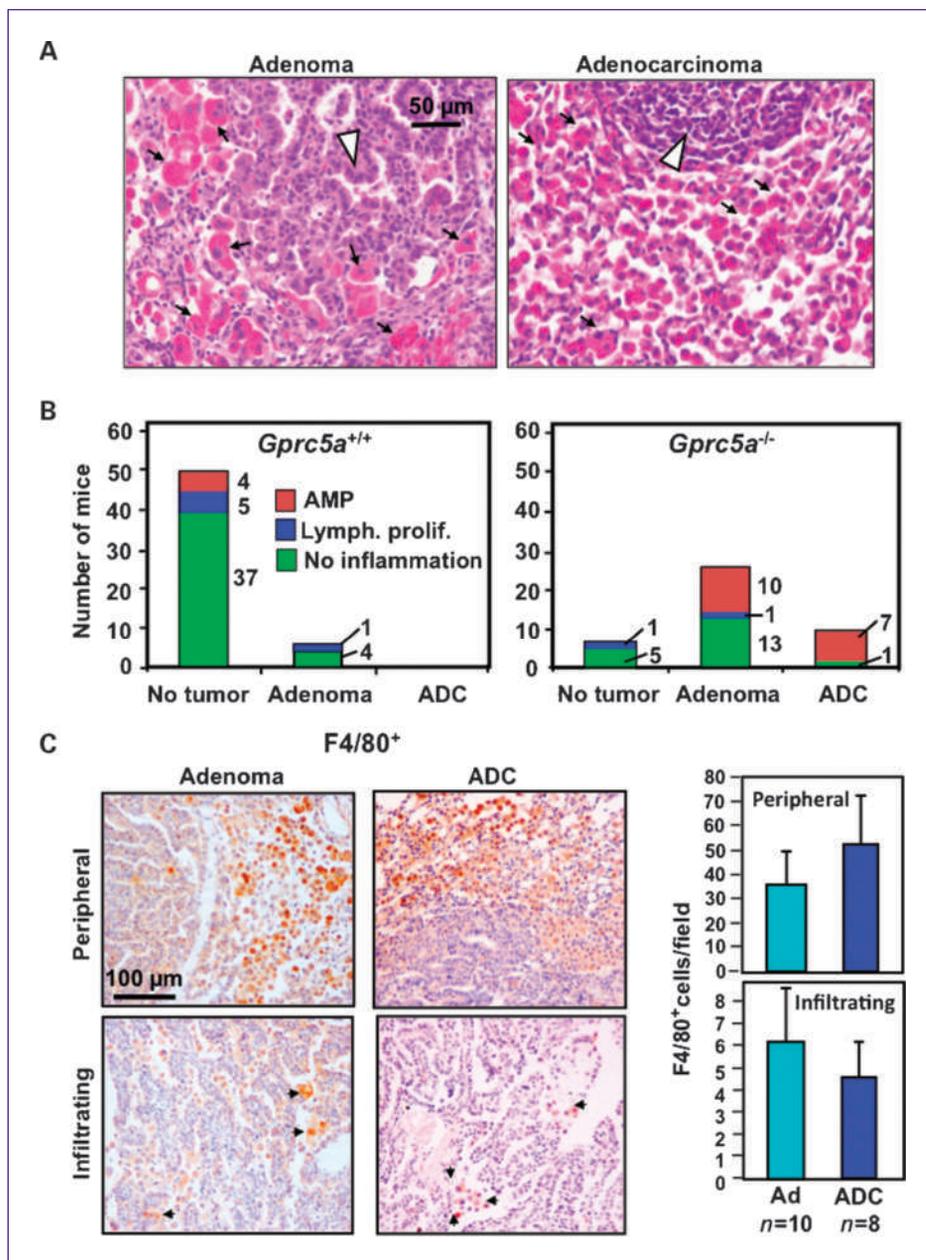[3] H. Kadara et al., submitted for publication.

Fig. 1. Relationships among macrophage pneumonia, lung tumors, and angiogenesis. A, photomicrographs of H&E-stained sections of an adenoma and an adenocarcinoma showing association of AMP with the epithelial tumor cells. B, quantitative analysis of the association of AMP with lung tumorigenesis. Tumor incidence is presented in relation to the presence of inflammatory cells in histologic sections of lungs of 51 Gprc5a^{+/+} mice (left) and 38 Gprc5a^{−/−} mice (right). The numbers near each bar represent mice in the corresponding category. The differences between Gprc5a^{+/+} and Gprc5a^{−/−} mice were statistically significant (Fisher's exact test) for the following: incidence of adenoma and/or adenocarcinoma (ADC), $P = 1 \times 10^{-6}$; adenoma incidence, $P = 1 \times 10^{-7}$; adenocarcinoma incidence, $P = 0.0007$; AMP incidence, $P = 8 \times 10^{-5}$. C, photomicrographs of histologic sections of an adenoma and an adenocarcinoma from Gprc5a^{−/−} mice stained with F4/80 antibodies for detection of mature macrophages in the periphery and within (infiltrating) tumors. The bar graphs (bottom, right) represent the mean number of F4/80^{+} cells in 10 adenomas (from 10 different mice) and 8 adenocarcinomas (from 7 different mice). Note that the values on the Y axis of the graph showing peripheral F4/80^{+} cells are much higher than in the graph showing data on infiltrating cells.

chemokines were higher by 20% to 515%, and one was lower by 36% in the lungs of Gprc5a^{−/−} relative to lungs of Gprc5a^{+/+} mice (Fig. 2A). With the exception of interleukin (IL)-5, all other 23 factors can be produced by monocytes/macrophages (http://www.copewithcytokines.de/cope.cgi?key=monocytes). Furthermore, 18 of these 24 factors (marked with an asterisk) are known targets of the transcription factor NF-κB, whereas 9 (marked with a pound sign) are NF-κB activators.

To determine whether Gprc5a^{−/−} mice respond differently than Gprc5a^{+/+} mice to inflammatory challenge, we treated both types of mouse with LPS, which stimulates

the production of TNFα by macrophages. Although low, the constitutive TNFα level in lung tissue of Gprc5a^{−/−} mice was 3-fold higher than in Gprc5a^{+/+} mice. LPS treatment increased the level of TNFα in both mouse genotypes by ~3 fold (Fig. 2B). Moreover, LPS treatment increased the level of Ym1, a chitinase-like secretory protein that is induced in alternatively activated macrophages (M2) regulated by IL-13 during inflammation, in the lungs of Gprc5a^{−/−} mice but not in Gprc5a^{+/+} mice as indicated by Western blotting (Fig. 2B, bottom left).

To determine whether LPS treatment also activated NF-κB differentially in lungs of Gprc5a^{+/+} and Gprc5a^{−/−}

mice, we used EMSA to analyze nuclear extracts of total lung homogenates prepared 4 hours after i.p. injection of LPS. Figure 2C shows that LPS induced NF-κB binding to DNA consensus sequence in the lungs of *Gprc5a*$^{-/-}$ to a much higher level than in *Gprc5a*$^{+/+}$ mice. Although the cell type(s) in which this increased NF-κB activation has taken place is not clear because we prepared nuclear extracts from whole lung homogenates, an immunohistochemical analysis of lung sections for p65 localization 4 hours after LPS treatment showed more extensive translocation of cytoplasmic p65 protein into the nuclei of bronchiolar epithelial cells in lungs of *Gprc5a*$^{-/-}$ mouse than in *Gprc5a*$^{+/+}$ mouse lungs (Fig. 2D). These results show that deletion of the *Gprc5a* gene enhances NF-κB activation by

LPS in mouse lungs *in vivo* and that at least some of the activation occurs in lung epithelial cells.

Enhanced *in vitro* proliferation and survival of lung epithelial cells isolated from tracheas of *Gprc5a*$^{-/-}$ compared with *Gprc5a*$^{+/+}$ mouse lungs

Because the lungs contain multiple cell types, both epithelial and mesenchymal, which interact with each other through direct contact or via soluble secreted factors, we wondered whether the loss of *Gprc5a* in epithelial cells leads to aberrant NF-κB activation also when the cells are in a homogeneous culture *in vitro*. Therefore, we established epithelial cell lines from lung tracheas. Both *Gprc5a*$^{+/+}$ and *Gprc5a*$^{-/-}$ cultured cells exhibited an epithelial morphology (Fig. 3A);
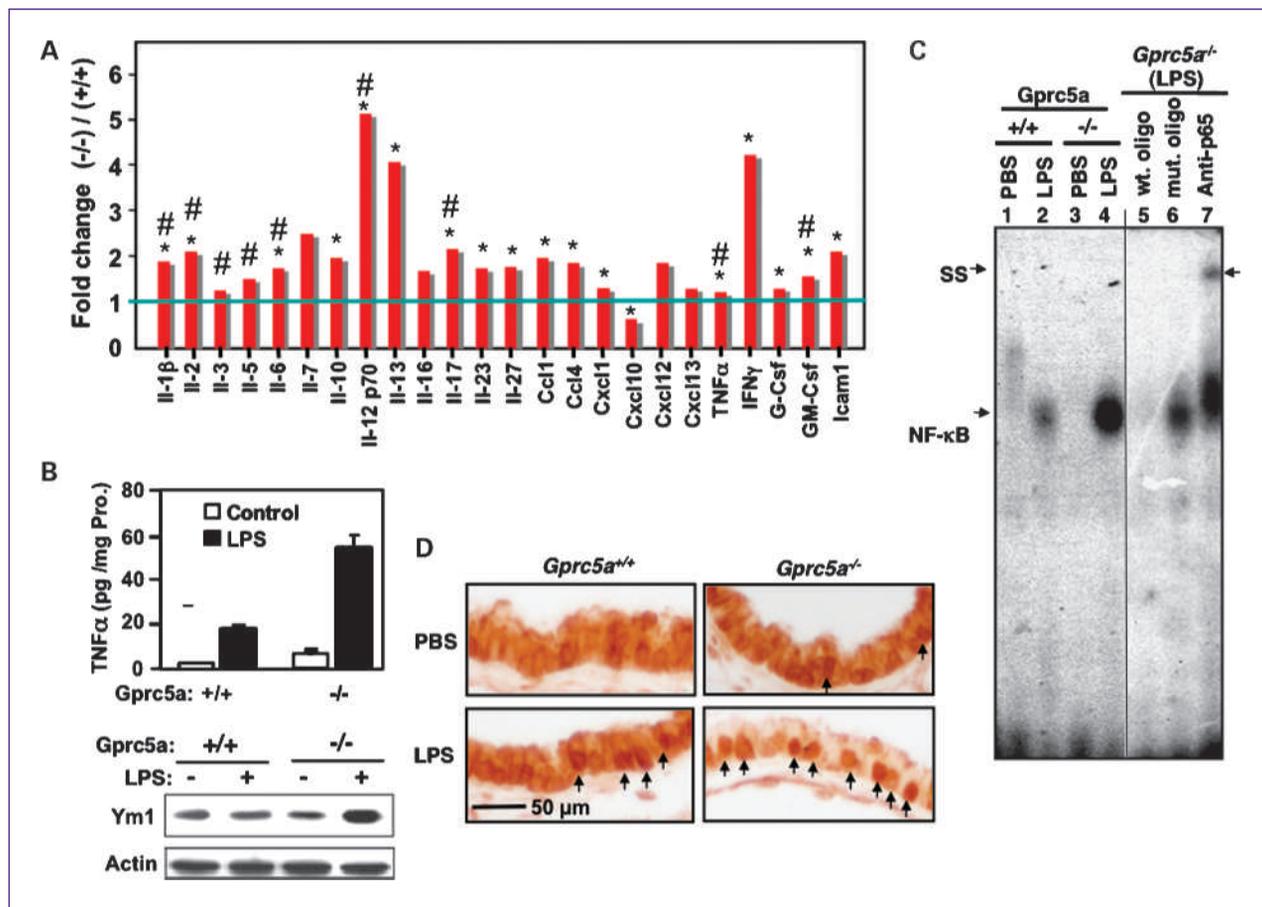

Fig. 2. Expression of inflammatory cytokines in lung tissues from *Gprc5a*$^{-/-}$ and *Gprc5a*$^{+/+}$ mice and the effects of LPS treatment *in vivo* on NF-κB activation. A, differential expression of cytokines and chemokines in extracts from *Gprc5a*$^{+/+}$ and *Gprc5a*$^{-/-}$ mouse lung homogenates determined by an immobilized antibody array. The signs * and # above some of the bars represent NF-κB targets and NF-κB activators, respectively. In addition to the indicated 24 analytes, the following 16 cytokines and chemokines showed <15% difference between the two samples and were not included in the graph (Il-1α, Il-1ra, Il-4, Ccl2, Ccl3, Ccl5, Ccl11, Ccl12, Ccl17, Cxcl9, Cxcl11, Kc, Timp-1, Term-1, M-Csf, and C5a). B, bar graph, TNFα levels in lung tissue homogenates of *Gprc5a*$^{+/+}$ and *Gprc5a*$^{-/-}$ mice measured by ELISA using samples collected 4 h after i.p. injection of LPS or PBS. Bottom left, immunoblot of lung homogenates from control and LPS-treated *Gprc5a*$^{+/+}$ and *Gprc5a*$^{-/-}$ mice using antibodies against Ym1 and actin. C, lanes 1 to 4, EMSA for detection of NF-κB DNA-binding proteins in nuclear extracts prepared from lung tissue homogenates of *Gprc5a*$^{+/+}$ and *Gprc5a*$^{-/-}$ mice treated with PBS or LPS as above. Nuclear extracts from lungs of LPS-treated *Gprc5a*$^{-/-}$ mice were also used to analyze the specificity of the EMSA by interference with NF-κB binding to consensus binding site using either wild-type (lane 5) or mutant (lane 6) oligonucleotides as competitors. Lane 7, the presence of p65 in the shifted complex was analyzed by adding anti-p65 antibodies to the EMSA reaction to induce a supershifted complex (SS). D, photomicrographs of histologic sections of lung tissues collected from *Gprc5a*$^{+/+}$ and *Gprc5a*$^{-/-}$ mice 4 h after i.p. injection of LPS or PBS and stained using antibodies against the p65 subunit of NF-κB to detect its translocation into the nucleus. Arrows point to positive nuclei.

however, their growth patterns were distinct. The $Gprc5a^{+/+}$ cells were contact inhibited after reaching a confluent state, and most of the cultures had undergone senescence after five to seven passages. In contrast, the $Gprc5a^{-/-}$ cells continued to proliferate after confluence and reached high densi-ties. The expected differential expression of $Gprc5a$ mRNA and protein in the cultured cells was shown by RT-PCR and immunoblotting (Fig. 3B). However, no differences were found between the two cell lines in the expression of the NF-κB subunit p65 or the NF-κB inhibitor IκBα (Fig. 3B).
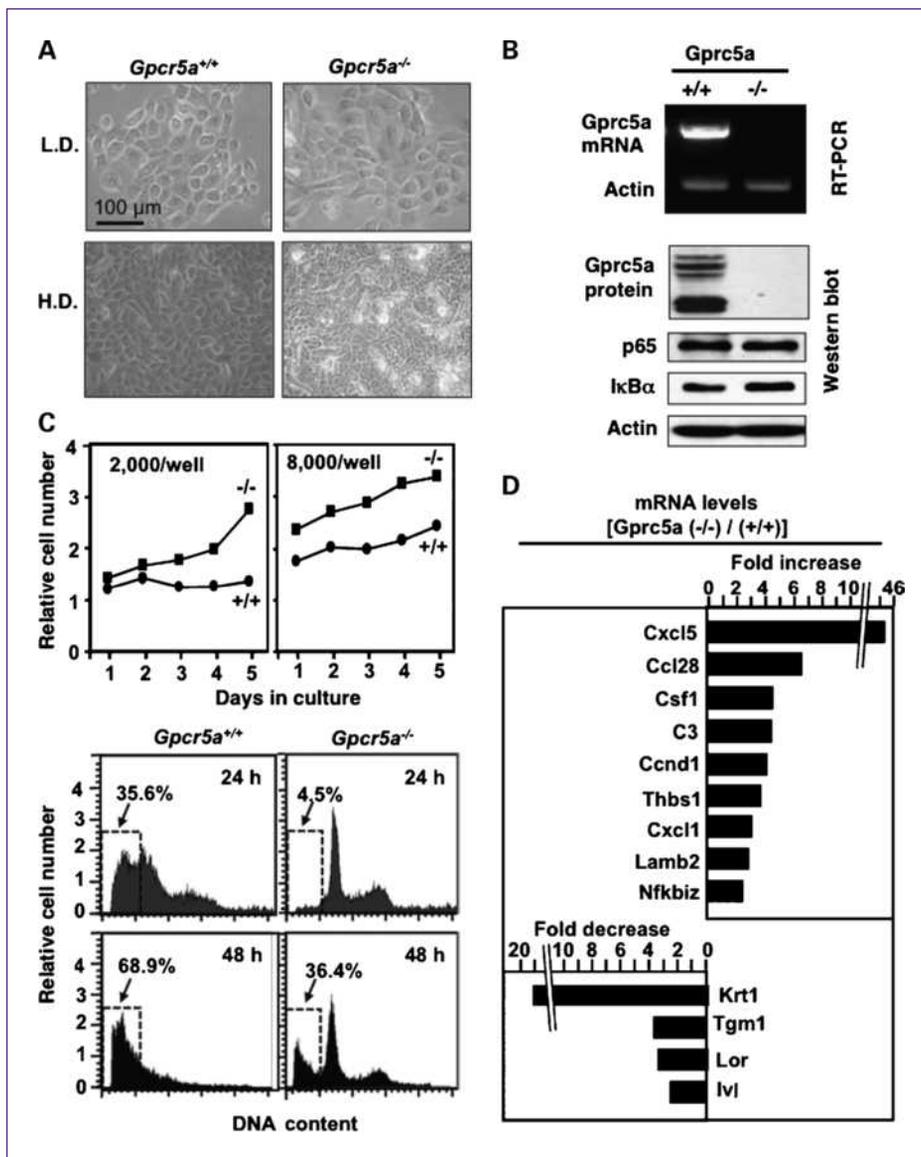

Fig. 3. Characteristics of epithelial cells cultured from tracheas of $Gprc5a^{+/+}$ and $Gprc5a^{-/-}$ mice. A, photomicrographs of low-density (L.D.) and high-density (H.D.) cell cultures taken using a phase-contrast microscope. B, expression of $Gprc5a$ mRNA (RT-PCR) and protein (Western blot) and NF-κB subunit p65, IκBα, and actin (Western blot) in the above cells. C, line graph, growth curves of $Gprc5a^{+/+}$ and $Gprc5a^{-/-}$ cells seeded in 96-well plates at 2×10^3 and 8×10^3 per well and analyzed daily for 5 d using a MTT assay to estimate cell numbers. Points, mean of triplicate cultures; bars, SD. Bottom, left, fluorescence-activated cell sorting analysis of DNA content of cells stained with propidium iodide 24 and 48 h after suspending them over PolyHEMA-coated tissue culture wells to induce anoikis. The sub-G_1 cell population is indicated by dotted line boxes. The numbers above the boxes indicate the percentage of dead cells within the cell population. D, differential expression of NF-κB target genes (top) and squamous differentiation markers (bottom) identified by mining our data on gene expression microarray analysis of mRNA from the above cells.[3] The full names of the genes and the P value for the significance of the difference in their expression level (univariate t test with random variance) in $Gprc5a^{+/+}$ and $Gprc5a^{-/-}$ cells are as follows: Cxcl5, chemokine (C-X-C motif) ligand 5 ($P < 10^{-7}$); Ccl28, chemokine (C-C motif) ligand 28 ($P < 10^{-7}$); Csf1, colony-stimulating factor 1 (macrophage; $P < 10^{-7}$); C3, complement component 3 ($P = 9 \times 10^{-7}$); Ccnd1, cyclin D1 ($P < 10^{-7}$); Thbs1, thrombospondin 1 ($P = 6 \times 10^{-7}$); Cxcl1, chemokine (C-X-C motif) ligand 1 ($P = 2.3 \times 10^{-6}$); Lamb2, laminin β2 ($P = 2.04 \times 10^{-5}$); Nfkbiz, nuclear factor of κ light polypeptide gene enhancer in B-cell inhibitor ζ ($P = 4 \times 10^{-7}$); Krt1, keratin 1 ($P < 10^{-7}$); Tgm1, transglutaminase I ($P = 9 \times 10^{-6}$); Lor, loricrin ($P = 9 \times 10^{-7}$); Ivl, involucrin ($P = 6 \times 10^{-7}$).
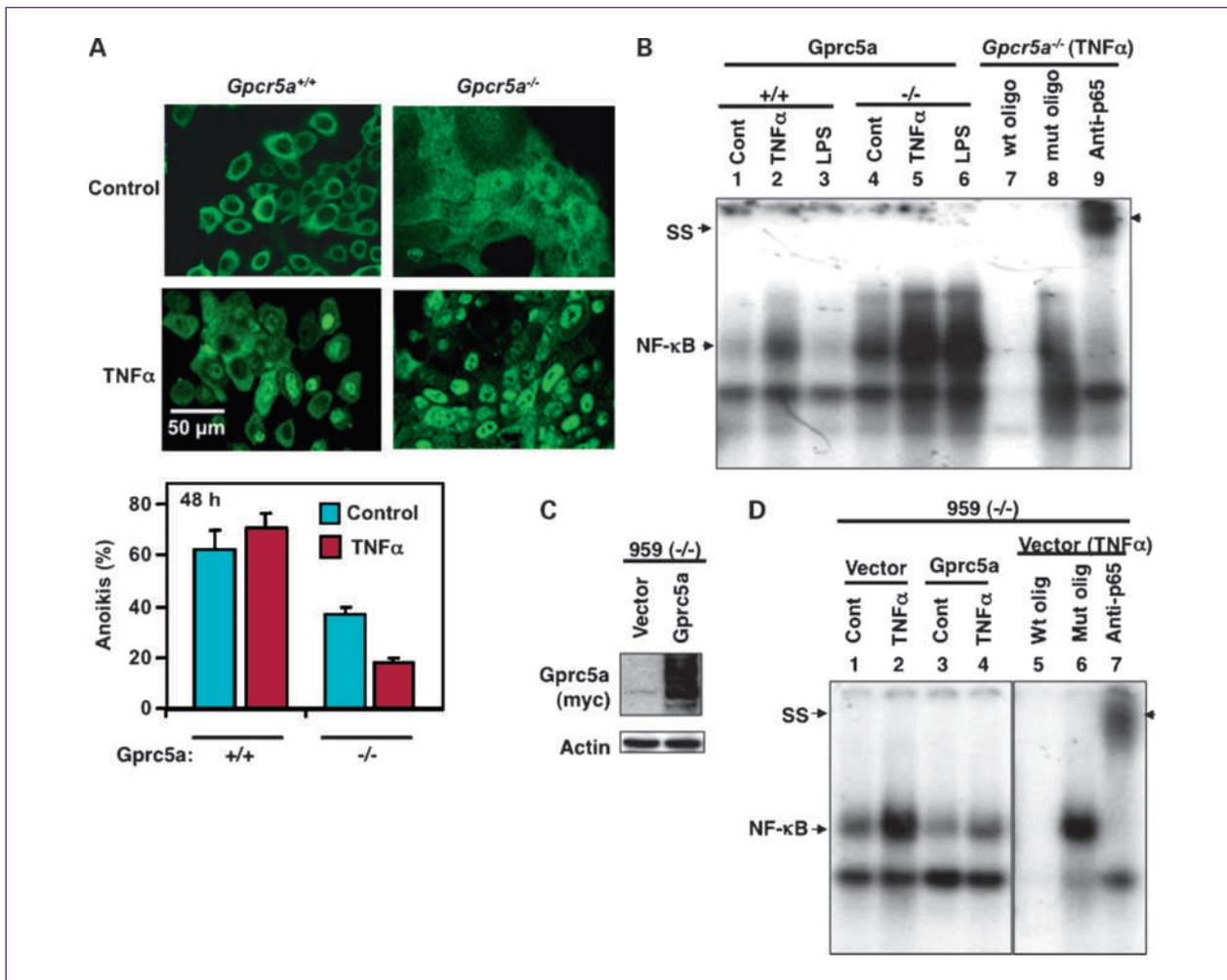
Fig. 4. Differential activation of NF-κB in *Gprc5a*$^{+/+}$ and *Gprc5a*$^{-/-}$ cells. A, localization of NF-κB subunit p65 in *Gprc5a*$^{+/+}$ and *Gprc5a*$^{-/-}$ cells after a 30-min exposure to TNFα (5 ng/mL) or control medium by immunofluorescent staining using anti-p65 primary antibodies and FITC-labeled secondary antibodies. Bottom left bar graph, anoikis was analyzed as described in Fig. 3C above in *Gprc5a*$^{+/+}$ and *Gprc5a*$^{-/-}$ cells treated with control medium or medium with TNFα (5 ng/mL) for 48 h in suspension over PolyHEMA-coated tissue culture wells. B, NF-κB activation in normal *Gprc5a*$^{+/+}$ and *Gprc5a*$^{-/-}$ lung cells detected by EMSA using nuclear extracts from cells harvested 30 min after treatment with TNFα (5 ng/mL), LPS (1 μg/mL), or control medium (Cont). Lanes 7 and 8, competition for NF-κB DNA binding using cold wild-type (wt) or mutant (mut) oligonucleotides (oligo) of the NF-κB–binding sequence. The ability of anti–NF-κB p65 antibodies to supershift (SS) the NF-κB complex is shown in lane 9. C, 959(–/–) adenocarcinoma cells were transfected with either vector only or a Myc-tagged *Gprc5a* expression vector and the expression of the protein was confirmed by Western blotting. D, NF-κB DNA-binding activities in transfected 959(–/–) cells detected by EMSA after treatment with TNFα or control medium as in B above.

The *Gprc5a*$^{+/+}$ cells required seeding at high initial density (e.g., 8,000 per well) to proliferate even if slowly (Fig. 3C). In contrast, the *Gprc5a*$^{-/-}$ cells were able to proliferate even when seeded at a lower density and then continued to grow indefinitely without undergoing senescence, thus behaving as spontaneously immortalized cells.

The above cells also exhibited differential sensitivity to induction of anoikis by denial of cell attachment. Specifically, 36% and 69% of *Gprc5a*$^{+/+}$ cells have died after incubation in PolyHEMA-coated tissue culture dishes for 24 and 48 hours, respectively, compared with only 4.5% and 36% death, respectively, in *Gprc5a*$^{-/-}$ cell cultures (Fig. 3C,

bottom left). These results indicated that *Gprc5a*$^{-/-}$ cells possess a higher proliferative capacity and higher resistance to anoikis than *Gprc5a*$^{+/+}$ cells. However, despite their ability to survive for a limited time under anchorage-independent conditions in liquid medium, the *Gprc5a*$^{-/-}$ cells had failed to form colonies in semisolid agar or to form tumors when injected either s.c. or into the tail vein of syngeneic mice, indicating that they are immortal but not transformed (data not shown). Indeed, no mutation was found in Trp53 (exons 5, 6, 7, or 8) or the Kras gene (exons 1 and 2).

Global gene expression analysis of the *Gprc5a*$^{-/-}$ and *Gprc5a*$^{+/+}$ cells done as a part of a separate study[3] provided
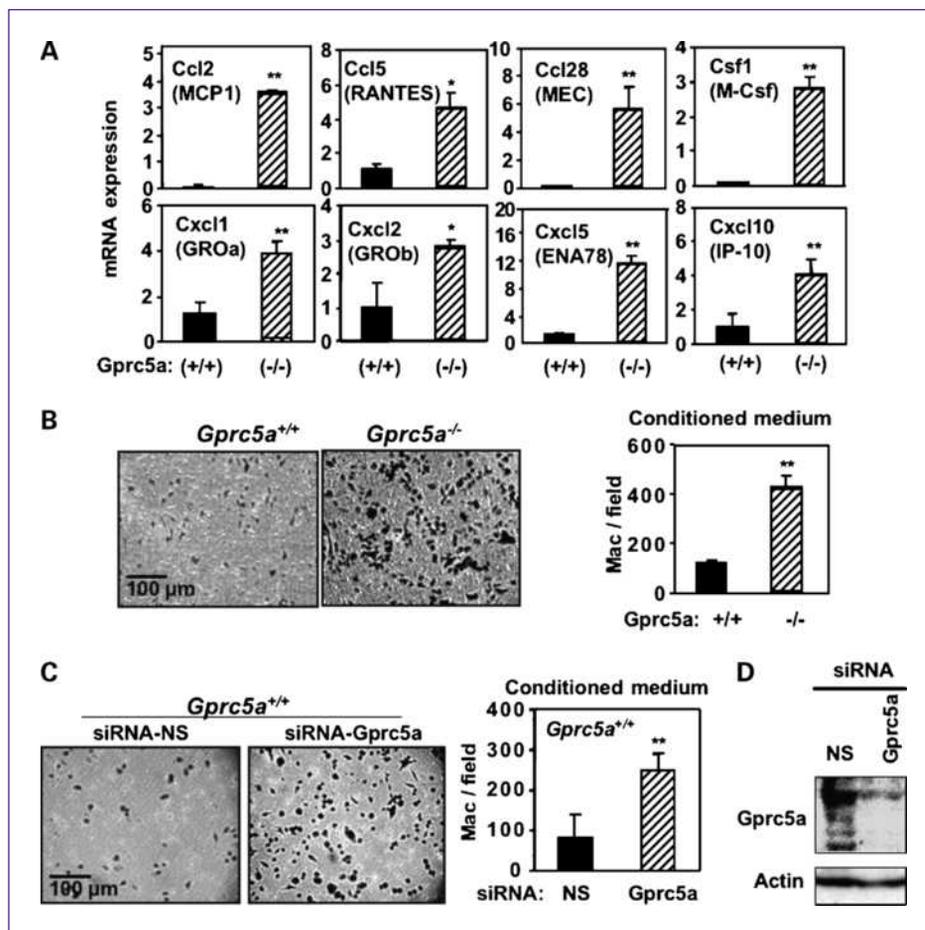
Fig. 5. Differential expression of chemokines and cytokines in cultured *Gprc5a*^{+/+} and *Gprc5a*^{−/−} cells and the effects of conditioned medium on macrophage migration. A, real-time PCR analysis of the indicated chemokines and cytokines using mRNA from cultured lung epithelial cells. The data represent the mean ± SE of triplicate measurements. B, analysis of the ability of conditioned medium of lung epithelial cells to promote macrophage migration. Left, MH-S cells that had migrated to the membrane underside were stained with crystal violet and photographed under the microscope. Right, the mean numbers of macrophages per field (±SD) were calculated after analyzing four fields. C, analysis of the macrophage migration-promoting activities of the conditioned medium of *Gprc5a*^{+/+} cells transiently transfected with siRNA against *Gprc5a* or with a nonspecific (NS) sequence. D, confirmation of the silencing of Gprc5a by the specific siRNA using immunoblotting of protein prepared from *Gprc5a*^{+/+} cells treated as in C. The significance of the differences between *Gprc5a*^{−/−} and *Gprc5a*^{+/+} in all above data is indicated by * ($P < 0.05$) and ** ($P < 0.001$, Student's *t* test).

an opportunity to mine the data for genes that are known targets of NF-κB. Figure 3D shows that the expression of the NF-κB target genes Cxcl5, Ccl28, Csf1, C3, Ccnd1, Thbs1, Cxcl1, Lamb2, and Nfκbiz was 2- to 45-fold higher in the *Gprc5a*^{−/−} cells than in the *Gprc5a*^{+/+} cells. In contrast, the expression of markers of squamous cell differentiation, including Krt1, Tgm1, Lor, and Ivl, was reduced in the *Gprc5a*^{−/−} cells compared with the *Gprc5a*^{+/+} cells by 2.8- to 18-fold (Fig. 3D).

Increased NF-κB activation in cells cultured from *Gprc5a*^{−/−} mouse lung

Immunofluorescent staining with anti-p65 antibodies (Fig. 4A) showed that without any treatment, p65 was localized primarily in the cytoplasm of *Gprc5a*^{+/+} cells (Fig. 4A, top left), whereas most *Gprc5a*^{−/−} cells showed both cytoplasmic and nuclear localization (Fig. 4A, top right), Exposure to TNFα induced p65 translocation from the cytoplasm to the nucleus in *Gprc5a*^{−/−} cells to a greater extent than in *Gprc5a*^{+/+} cells (Fig. 4A, bottom). TNFα treatment also exerted different effects on the sensitivity of the cells to anoikis. Whereas TNFα increased slightly the induction of anoikis in suspended *Gprc5a*^{+/+} cells, the

same treatment reduced the already lower anoikis in *Gprc5a*^{−/−} cells (Fig. 4A, bottom left bar graph).

Examination by EMSA of nuclear extracts of untreated, TNFα-treated, and LPS-treated *Gprc5a*^{+/+} and *Gprc5a*^{−/−} cells revealed that the basal NF-κB DNA-binding activity was much higher in *Gprc5a*^{−/−} than in *Gprc5a*^{+/+} cells ((Fig. 4B, lanes 4 and 1), respectively) and that TNFα increased NF-κB activation in *Gprc5a*^{+/+} cells to a level comparable with the basal level in untreated *Gprc5a*^{−/−} cells (Fig. 4A, lanes 2 and 4). A similar TNFα treatment of *Gprc5a*^{−/−} cells increased NF-κB activation above the basal already level (Fig. 4A, lanes 4 and 5). Furthermore, whereas LPS treatment failed to activate NF-κB in *Gprc5a*^{+/+} cells, it increased NF-κB activity in *Gprc5a*^{−/−} cells to a level similar to TNFα treatment (Fig. 4B, lanes 6 and 3), respectively. The specificity of the DNA-binding activity of NF-κB in the EMSA assay was confirmed by competition with access cold oligonucleotide and supershifting with anti-p65 antibodies (Fig. 4B, lanes 7-9).

To complement these loss-of-function data with gain-of-function results, we generated stable transfectants of 959(−/−) adenocarcinoma cell line using a Myc-tagged *Gprc5a* expression vector or a vector control (Fig. 4C) and

compared NF-κB activation by TNFα in these cells by EMSA. Figure 4D shows that expression of *Gprc5a* suppressed the basal NF-κB activity (compare lanes 1 and 3) and inhibited NF-κB activation by TNFα (Fig. 4D, lanes 2 and 4).

Enhanced induction of macrophage migration by medium conditioned by *Gprc5a*$^{-/-}$ compared with *Gprc5a*$^{-/-}$ cells

Because many NF-κB target genes play essential roles in inflammation (16, 17) and some mediate macrophage recruitment, we analyzed by quantitative PCR the expression of eight such genes, including four (*Ccl28*, *Csf1*, *Cxcl1*, and *Cxcl5*) that have been found to be upregulated in *Gprc5a*$^{-/-}$ cells by the global gene expression analysis (Fig. 3D). Figure 5A shows that the levels of the mRNAs of all eight genes were elevated in the *Gprc5a*$^{-/-}$ compared with *Gprc5a*$^{+/+}$ epithelial cells by 3- to 70-fold. Because some of these cytokines (e.g., Ccl2, Ccl5, and Csf1) are known to promote macrophage recruitment *in vivo*, we examined the

effects of conditioned serum-free medium from cultures of epithelial cells on the migration of mouse alveolar macrophage-like cell line MH-S and found that the medium of *Gprc5a*$^{-/-}$ cells induced the migration of four times as many macrophages as the medium of *Gprc5a*$^{+/+}$ cells (Fig. 5B). To assess whether Gprc5a was responsible for the observed differential induction of macrophage migration, we silenced *Gprc5a* expression by siRNA. The conditioned medium of *Gprc5a*$^{+/+}$ cells in which the gene was silenced exhibited an increased ability to induce macrophage migration (Fig. 5C and D).

Silencing of NF-κB p65 in *Gprc5a*$^{-/-}$ cells partially reverses their phenotype

To determine whether the increased expression of macrophage chemotactic factors was actually mediated by NF-κB in *Gprc5a*$^{-/-}$ cells, we silenced p65 by transient transfection with specific siRNA (Fig. 6A, Western blot). The suppression of NF-κB increased the sensitivity of the *Gprc5a*$^{-/-}$ cells to
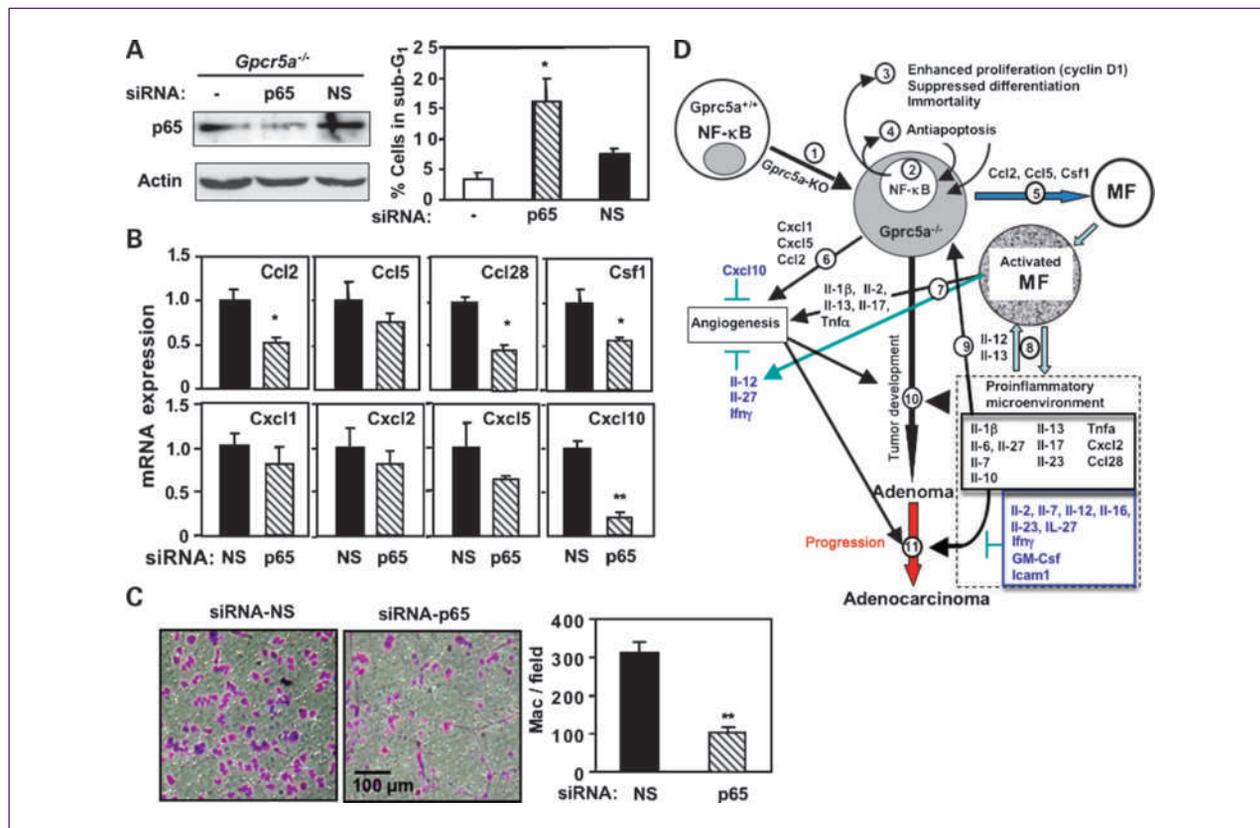

Fig. 6. Implication of NF-κB signaling in the aberrant phenotype of *Gprc5a*$^{-/-}$ cells. A, left, silencing of p65 in *Gprc5a*$^{-/-}$ cells transfected transiently with siRNA against p65 but not in cells transfected with nonspecific siRNA detected by immunoblotting. Right, effects of transfecting *Gprc5a*$^{-/-}$ cells with siRNA against p65 or nonspecific oligonucleotide on sub-G$_1$ cell population representing dead cells after a 24-h suspension was determined as in Fig. 3D. B, real-time PCR analysis of the indicated chemokines and cytokines using total RNA from *Gprc5a*$^{-/-}$ cells treated with p65-specific or nonspecific siRNA. Columns, mean of triplicate measurements; bars, SD. C, left, analysis of the ability of conditioned medium of *Gprc5a*$^{-/-}$ cells treated with siRNA to promote macrophage migration; right, columns, mean number of macrophages per field in four fields; bars, SD. The statistical significance of the differences between *Gprc5a*$^{-/-}$ cells transfected with p65-specific siRNA or nonspecific oligonucleotide is indicated by * ($P < 0.05$) and ** ($P < 0.001$, Student's t test). D, schema of the proposed sequence of events (indicated by numbers) resulting from *Gprc5a* loss in lung airway epithelial cells *in vivo*. The cytokines presented in black fonts stimulate and those in blue fonts inhibit angiogenesis or tumor development as indicated.

anoikis (Fig. 6A, bar graph) and also decreased the expression of several chemokines, including Ccl2, Ccl28, Csf1, and Cxcl10 (Fig. 6B). Small but statistically insignificant decreases were also noted in the levels of Cxcl5 and Ccl5. Importantly, the silencing of p65 decreased by 3-fold the ability of the conditioned medium of $Gprc5a^{-/-}$ cells to induce macrophage migration (Fig. 6C).

Discussion

Recently, we showed that $Gprc5a^{-/-}$ mice develop spontaneous lung tumors after a lag period lasting from 12 and 24 months (20). The reason for this prolonged time was not clear, but we surmised that the loss of $Gprc5a$ is not sufficient by itself for full transformation of the epithelial cell precursors of the tumors. However, the nature of the additional changes that presumably are needed for tumor development and what drives them during the latent period remained unknown. In this study, we found by retrospective analysis of histologic tumor specimens from the above study that many of the tumors in the $Gprc5a^{-/-}$ mouse lungs, especially the adenocarcinomas, were surrounded and infiltrated by macrophages. Because the migration of macrophages into the microenvironment of tumors is a frequent event and tumor-associated macrophages are known to secrete inflammatory factors that can promote lung tumor development and progression (13), we thought that the loss of $Gprc5a$ may be causally related to the attraction of macrophages into the lungs of knockout mice and that once there the macrophages create an inflammatory microenvironment providing the conditions for transformation and promotion of carcinogenesis (30).

By comparing and contrasting constitutive and TNFα- or LPS-induced inflammation-related proteins and transcripts using tissues and epithelial cell lines derived from lung tissues of $Gprc5a^{+/+}$ and $Gprc5a^{-/-}$ mice at an early age before tumors develop, as well as lung tumor specimens, we obtained data that support, at least partially, the model presented in Fig. 6D. According to this model, the loss of $Gprc5a$ in lung epithelial cells triggers at least three processes: one intrinsic process that leads to cell autonomy, and the other two extrinsic processes that create an inflammatory, angiogenic, and protumorigenic microenvironment. We further propose that these processes cooperate to promote oncogenesis. The schema in Fig. 6D is "idealized" in that it depicts a series of steps in the process (numbered in Fig. 6D), although specimens used to generate our in vivo data were collected at specific time points and do not represent the dynamics of the processes involved and many of the steps may be concurrent rather than sequential.

We propose that $Gprc5a$ loss (Fig. 6D, step 1) leads to lung carcinogenesis by the following interrelated steps: NF-κB activation and increased expression of target genes in the lung epithelial cells (Fig. 6D, step 2) that enhance proliferation potential, survival, and immortalization of the epithelial cells (Fig. 6D, steps 3 and 4). The secretion of NF-κB–regulated chemokines and cytokines by the $Gprc5a^{-/-}$ lung cells can lead to recruitment of macrophages (Fig. 6D, step 5) and to induction of angiogenesis (Fig. 6D, step 6). The macrophages produce and secrete into the microenvironment a variety of cytokines, chemokines, and growth factors (Fig. 6D, steps 7-9) that can enhance angiogenesis (Fig. 6D, step 7) and also act directly on the lung epithelial cells to enhance the development of adenomas and their progression to adenocarcinomas (Fig. 6D, steps 9-11). The finding that silencing of p65 in $Gprc5a^{-/-}$ cells partially decreased their resistance to anoikis and their ability to stimulate macrophage migration indicated that NF-κB activation might mediate many of the phenotypic characteristics that distinguish the $Gprc5a^{-/-}$ cells from their wild-type counterparts. It is important to note that we cannot exclude the possibility that some of the phenotypic characteristics of the cultured $Gprc5a$ lung cells may have been acquired by unintended selection during the in vitro establishment of the cell line from primary tracheal cells.

It is noteworthy that Cxcl10 produced by the $Gprc5a^{-/-}$ lung cells can potentially inhibit angiogenesis. In addition, some of the cytokines identified in the lung homogenates of $Gprc5a^{-/-}$ mice can suppress tumorigenesis (indicated in Fig. 6D in blue fonts), whereas other factors can exert both protumorigenic and antitumorigenic effects depending on their concentration. Many of these factors could have been produced by macrophages with distinct properties ranging from the classically activated M1 to the alternatively activated M2, which are known to produce factors with potentially opposing effects (31). The increase in the level of the M2 macrophage marker Ym1 (chitinase) protein observed after LPS treatment in the lungs of $Gprc5a^{-/-}$ but not of $Gprc5a^{+/+}$ mice indicates that more protumorigenic M2 macrophages can be attracted to lungs of LPS-treated $Gprc5a^{-/-}$ mice or that alveolar macrophages already present in the lungs of such mice are more readily differentiated into M2 macrophages. The presence of different cell types and cytokines with potentially opposing effects is quite common in tumor microenvironments, and it is the spatiotemporal balance of the proangiogenic and antiangiogenic factors and the protumorigenic and antitumorigenic factors in specific sites that eventually determines whether tumors will develop or not (12).

The exact mechanisms by which the macrophages and the inflammatory microenvironment enhance carcinogenesis in our $Gprc5a$ knockout mouse model are not clear. Tumor-associated macrophages are known to release a plethora of growth factors, cytokines, chemokines, and enzymes and reactive oxygen intermediates that enhance epithelial cell growth as well as causing genetic instability by DNA damage, and increase angiogenesis and cell invasiveness (13, 17, 31–33).

Although inflammation is known to increase angiogenesis (32, 34), we found no enhancing effect of low and moderate grade of AMP on angiogenesis in adenomas and adenocarcinomas from $Gprc5a^{-/-}$ mice, whereas the high-grade AMP actually inhibited angiogenesis. A likely explanation is that high levels of proangiogenic Cxcl5, Cxcl1, and Ccl2 released by the $Gprc5a^{-/-}$ epithelial cells

are sufficient to induce and maintain angiogenesis despite the production by the same cells of lower levels of the angiostatic Cxcl10 and independently of any proangiogenic or antiangiogenic signals from macrophages. Notably, Cxcl5 is the most highly differentially expressed chemokine between $Gprc5a^{-/-}$ and $Gprc5a^{+/+}$ epithelial cells. This finding is interesting and relevant to human lung cancer because the human orthologous gene *CXCL5* has been previously found to be upregulated in human non–small cell lung carcinoma by cyclooxygenase-2 via NF-κB activation (35) and has been implicated as an angiogenic factor in the development of non–small cell lung carcinomas and as a marker of poor prognosis in non–small cell lung carcinoma patients (36).

Our emphasis on the possible role of inflammation stems from the finding that 7 of 8 adenocarcinomas and 10 of 24 adenomas were associated with AMP, suggesting that the presence of macrophages in the microenvironment may be important for the development of adenomas and for their progression to adenocarcinoma. However, because we have also found that 14 of 24 adenomas and 1 of 8 adenocarcinomas had developed without associated macrophages, it seems that at least a subset of adenomas can develop independently of macrophages.

The enhancement of lung carcinogenesis by inflammation has been shown in several mouse models mostly involving exposure to carcinogens (3, 4). The role of lung epithelial cells in the inflammation has not received much attention until recently. The use of targeted expression of mutant Kras in bronchiolar epithelial cells in mouse lungs was found to induce inflammatory response with extensive infiltration of macrophages and neutrophils (37). In this model, the bronchiolar epithelial cells produced some of the same cytokines that were identified in our study, notably Cxcl1 and Cxcl5. However, the early mortality (median survival of 8 weeks) resulting from the robust inflammatory response in the Kras model was not seen in our study and our mice survived for 12 to 24 months. The reason for this difference is not clear.

Our finding that the $Gprc5a^{-/-}$ lung epithelial cells have a constitutively active nuclear p65 and are more responsive to NF-κB activation by TNFα and LPS relative to $Gprc5a^{+/+}$ cells is a novel result. The transcription of several NF-κB target genes was also elevated in the $Gprc5a^{-/-}$ cells including cyclin D1 that could mediate enhancement of cell proliferation and increased survival under proapoptotic stress. The increased expression of cyclin D1 has been associated with enhanced growth of mouse lung premalignant and tumor cells *in vitro* and *in vivo* and has been proposed as a target for chemoprevention (38, 39). Interestingly, targeted p65 overexpression in mouse lung epithelial cells in transgenic mice caused proliferation of these cells in embryo lungs and protected them against apoptosis as did LPS treatment of wild-type mice through activation of NF-κB (40).

Not only immune cells but also normal lung airway epithelial cells and lung cancer cells can produce a variety of cytokines, many of which are regulated by NF-κB and contribute to the development of chronic lung inflammation

(28, 37, 41, 42). For example, the state of NF-κB activation in bronchioalveolar epithelial cells in several mouse strains was the overriding factor in determining the link between susceptibility to inflammation and lung cancer (43). Direct evidence for the pivotal roles of NF-κB activation in airway epithelial cells in induction of an inflammatory response and in promoting lung tumorigenesis has been shown only recently in an ethyl carbamate (urethane)–induced lung carcinogenesis model (44). Many of the cytokines and chemokines such as TNFα and IL-12 p70 identified in the lungs of our untreated $Gprc5a^{-/-}$ mice were also increased in the urethane-treated wild-type mice (44). Targeted expression of a dominant inhibitor of NF-κB in the airway epithelial cells *in vivo* decreased urethane-induced inflammation and tumor formation, indicating the importance of early activation of NF-κB signaling in airway epithelial cells in urethane-induced tumorigenesis (44). A similar approach of *in vivo* inhibition of NF-κB activation was used recently to show the importance of NF-κB signaling in a lung carcinogenesis model based on a combination of mutant Kras knock-in and Trp53 deletion without any carcinogen treatment (45). The latter study has shown that NF-κB activation in primary mouse embryo fibroblasts required a concomitant activation of mutant Kras (G12D) and a loss of Trp53 but did not occur in cells with only one of these changes. Restoration of wild-type Trp53 expression in mouse lung adenocarcinoma cells with oncogenic Kras and Trp53 deletion showed inhibition of nuclear localization of the NF-κB subunit p65. The changes in NF-κB activation depending on Kras and Trp53 status were correlated with apoptosis *in vitro* and suppression of tumor development and growth *in vivo* (45). Our model is distinct from the above two in that we achieved NF-κB activation in the lung epithelial cells by deletion of the *Gprc5a* gene, and such a deletion also enhanced LPS-induced activation of NF-κB in lung airway cells *in vivo*. We found no mutations in either Kras or Trp53 in the cultured $Gprc5a^{-/-}$ epithelial cells. Thus, it seems that wild-type Trp53 does not inhibit NF-κB activation in these cells. However, we cannot exclude a role for aberrations in Trp53 signaling pathway downstream of Trp53 in NF-κB activation in the $Gprc5a^{-/-}$ cells because functional and pathway analyses (Ingenuity Pathway Analysis) of the differentially expressed gene features between $Gprc5a^{-/-}$ and $Gprc5a^{+/+}$ cells revealed a significant modulation of gene sets associated with Trp53 signaling.[3]

The $Gprc5a^{-/-}$ mouse model exhibits similarities to several inflammation-related aspects of human lung carcinogenesis. For example, the activation of NF-κB observed in the $Gprc5a^{-/-}$ cells and the higher response to LPS *in vivo* are similar to the reports on increased numbers of cells with nuclear p65 staining in bronchial biopsies taken from smokers with normal lung function or from smokers with chronic obstructive pulmonary disease, an inflammation-driven pathology that increases the risk to develop lung cancer, compared with biopsies from nonsmokers (46). Moreover, nearly all of the cytokines and chemokines found to be upregulated in the $Gprc5a^{-/-}$

compared with $Gprc5a^{+/+}$ cells and the lung homogenates of $Gprc5a^{-/-}$ and $Gprc5a^{+/+}$ mice are increased in chronic obstructive pulmonary disease patients' lungs compared with nonsmokers' lungs (47). In addition, aberrant activation of NF-κB has been reported in the majority of human adenocarcinomas and precursor lesions, including atypical adenomatous hyperplasia, compared with normal epithelium (48).

The mechanism by which the loss of $Gprc5a$ in the knockout mouse and in the isolated tracheal epithelial cells leads to activation of NF-κB signaling is not clear. Previously, other G protein–coupled receptors have been found to stimulate inflammation by serving as receptors for a variety of chemokines (49) or by enhancing NF-κB signaling through activation of signaling upstream of NF-κB (50). However, activation of the β-adrenergic receptor by isoproterenol has been found to suppress NF-κB activation. The mechanism proposed for this effect was enhancement by the G protein–coupled receptor of the stabilizing interaction between β-arrestin2 and the endogenous NF-κB inhibitory protein IκBα, which prevents the nuclear translocation of cytoplasmic p65 (51). It is possible that Gprc5a inhibits NF-κB activation by a similar mechanism.

In conclusion, we have shown that the loss of the lung-specific tumor suppressor $Gprc5a$ leads to activation of NF-κB in lung epithelial cells in $vivo$ and in $vitro$, leading to autonomous cell growth as well as enhancement of inflammatory microenvironment, which seem to contribute to the lung tumorigenesis process in this new model of lung cancer. The model should be useful for assessment of the chemopreventive potential of agents targeting the microenvironment, including anti-inflammatory agents, inhibitors of macrophage function, and NF-κB inhibitors (9, 10, 52–54).

Disclosure of Potential Conflicts of Interest

No potential conflicts of interest were disclosed.

Grant Support

References

1. Jemal A, Siegel R, Ward E, et al. Cancer statistics. CA Cancer J Clin 2009;59:225–49.
2. Engels EA. Inflammation in the development of lung cancer: epidemiological evidence. Expert Rev Anticancer Ther 2008;8:605–15.
3. Malkinson AM. Role of inflammation in mouse lung tumorigenesis. Exp Lung Res 2005;31:57–82.
4. Bauer AK, Rondini EA. Review paper: the role of inflammation in mouse pulmonary neoplasia. Vet Pathol 2009;46:369–90.
5. Alberg AJ, Samet JM. Epidemiology of lung cancer. Chest 2003;123: 21–49S.
6. Punturieri A, Szabo E, Croxton TL, Shapiro SD, Dubinett SM. Lung cancer and chronic obstructive pulmonary disease: needs and opportunities for integrated research. J Natl Cancer Inst 2009;101: 554–9.
7. Yao H, Rahman I. Current concepts on the role of inflammation in COPD and lung cancer. Curr Opin Pharmacol 2009;9:375–83.
8. Stayner L, Smith R, Bailer J, et al. Exposure-response analysis of risk of respiratory disease associated with occupational exposure to chrysotile asbestos. Occup Environ Med 1997;54:646–52.
9. Moghaddam SJ, Barta P, Mirabolfathinejad SG, et al. Curcumin inhibits COPD-like airway inflammation and lung cancer progression in mice. Carcinogenesis 2009;30:1949–56.
10. Tyagi A, Singh RP, Ramasamy K, et al. Growth inhibition and regression of lung tumors by silibinin: modulation of angiogenesis by macrophage-associated cytokines and nuclear factor-κB and signal transducers and activators of transcription 3. Cancer Prev Res 2009; 2:74–83.
11. Slatore CG, Au DH, Littman AJ, Satia JA, White E. Association of nonsteroidal anti-inflammatory drugs with lung cancer: results from a large cohort study. Cancer Epidemiol Biomarkers Prev 2009;18: 1203–7.
12. Witz IP. Yin-yang activities and vicious cycles in the tumor microenvironment. Cancer Res 2008;68:9–13.
13. Solinas G, Germano G, Mantovani A, Allavena P. Tumor-associated macrophages (TAM) as major players of the cancer-related inflammation. J Leukoc Biol 2009;86:1065–73.

14. Albini A, Sporn MB. The tumor microenvironment as a target for chemoprevention. Nat Rev Cancer 2007;7:139–47.
15. Peebles KA, Lee JM, Mao JT, et al. Inflammation and lung carcinogenesis: applying findings in prevention and treatment. Expert Rev Anticancer Ther 2007;7:1405–21.
16. Vallabhapurapu S, Karin M. Regulation and function of NF-κB transcription factors in the immune system. Annu Rev Immunol 2009; 27:693–733.
17. Hallam S, Escorcio-Correia M, Soper R, Schultheiss A, Hagemann T. Activated macrophages in the tumour microenvironment—dancing to the tune of TLR and NF-κB. J Pathol 2009;219:143–52.
18. Cheng Y, Lotan R. Molecular cloning and characterization of a novel retinoic acid-inducible gene that encodes a putative G protein-coupled receptor. J Biol Chem 1998;273:35008–15.
19. Tao Q, Cheng Y, Clifford J, et al. Characterization of the murine orphan G-protein-coupled receptor gene Rai3 and its regulation by retinoic acid. Genomics 2004;83:270–80.
20. Tao Q, Fujimoto J, Men T, et al. Identification of the retinoic acid-inducible Gprc5a as a new lung tumor suppressor gene. J Natl Cancer Inst 2007;99:1668–82.
21. Murray AB, Luz A. Acidophilic macrophage pneumonia in laboratory mice. Vet Pathol 1990;27:274–81.
22. Nikitin AY, Alcaraz A, Anver MR, et al. Classification of proliferative pulmonary lesions of the mouse: recommendations of the mouse models of human cancers consortium. Cancer Res 2004;64:2307–16.
23. Hoenerhoff MJ, Starost MF, Ward JM. Eosinophilic crystalline pneumonia as a major cause of death in 129S4/SvJae mice. Vet Pathol 2006;43:682–8.
24. Deng J, Kloosterboer F, Xia W, et al. The NH(2)-terminal and conserved region 2 domains of adenovirus E1A mediate two distinct mechanisms of tumor suppression. Cancer Res 2002;62:346–50.
25. Bretland AJ, Lawry J, Sharrard RM. A study of death by anoikis in cultured epithelial cells. Cell Prolif 2001;34:199–210.
26. Mbawuike IN, Herscowitz HB. MH-S, a murine alveolar macrophage cell line: morphological, cytochemical, and functional characteristics. J Leukoc Biol 1989;46:119–27.

27. Sankaran K, Herscowitz HB. Phenotypic and functional heterogeneity of the murine alveolar macrophage-derived cell line MH-S. J Leukoc Biol 1995;57:562–8.

28. Zhong L, Roybal J, Chaerkady R, et al. Identification of secreted proteins that mediate cell-cell interactions in an *in vitro* model of the lung cancer microenvironment. Cancer Res 2008;68:7237–45.

29. Lee SH, Starkey PM, Gordon S. Quantitative analysis of total macrophage content in adult mouse tissues. Immunochemical studies with monoclonal antibody F4/80. J Exp Med 1985;161:475–89.

30. Colotta F, Allavena P, Sica A, Garlanda C, Mantovani A. Cancer-related inflammation, the seventh hallmark of cancer: links to genetic instability. Carcinogenesis 2009;30:1073–81.

31. Pelegrin P, Surprenant A. Dynamics of macrophage polarization reveal new mechanism to inhibit IL-1β release through pyrophosphates. EMBO J 2009;28:2114–27.

32. Lin EY, Pollard JW. Tumor-associated macrophages press the angiogenic switch in breast cancer. Cancer Res 2007;67:5064–6.

33. O'Byrne KJ, Dalgleish AG. Chronic immune activation and inflammation as the cause of malignancy. Br J Cancer 2001;85:473–83.

34. Albini A, Tosetti F, Benelli R, Noonan DM. Tumor inflammatory angiogenesis and its chemoprevention. Cancer Res 2005;65:10637–41.

35. Põld M, Zhu LX, Sharma S, et al. Cyclooxygenase-2-dependent expression of angiogenic CXC chemokines ENA-78/CXC ligand (CXCL) 5 and interleukin-8/CXCL8 in human non-small cell lung cancer. Cancer Res 2004;64:1853–60.

36. White ES, Flaherty KR, Carskadon S, et al. Macrophage migration inhibitory factor and CXC chemokine expression in non-small cell lung cancer: role in angiogenesis and prognosis. Clin Cancer Res 2003;9:853–60.

37. Ji H, Houghton AM, Mariani TJ, et al. Kras activation generates an inflammatory response in lung tumors. Oncogene 2006;25:2105–12.

38. Mamay CL, Schauer IE, Rice PL, et al. Cyclin D1 as a proliferative marker regulating retinoblastoma phosphorylation in mouse lung epithelial cells. Cancer Lett 2001;168:165–72.

39. Petty WJ, Dragnev KH, Dmitrovsky E. Cyclin D1 as a target for chemoprevention. Lung Cancer 2003;41:155–61.

40. Londhe VA, Nguyen HT, Jeng JM, et al. NF-κB induces lung maturation during mouse lung morphogenesis. Dev Dyn 2008;237: 328–38.

41. Fukuyama T, Ichiki Y, Yamada S, et al. Cytokine production of lung cancer cell lines: correlation between their production and the inflammatory/immunological responses both *in vivo* and *in vitro*. Cancer Sci 2007;98:1048–54.

42. Poynter ME, Irvin CG, Janssen-Heininger YM. A prominent role for airway epithelial NF-κB activation in lipopolysaccharide-induced airway inflammation. J Immunol 2003;170:6257–65.

43. Dahabre J, Vasilaki M, Stathopoulos GP, et al. Surgical management in lung metastases from colorectal cancer. Anticancer Res 2007;27: 4387–90.

44. Stathopoulos GT, Sherrill TP, Cheng DS, et al. Epithelial NF-κB activation promotes urethane-induced lung carcinogenesis. Proc Natl Acad Sci U S A 2007;104:18514–9.

45. Meylan E, Dooley AL, Feldser DM, et al. Requirement for NF-κB signalling in a mouse model of lung adenocarcinoma. Nature 2009;462: 104–7.

46. Di Stefano A, Caramori G, Oates T, et al. Increased expression of nuclear factor-κB in bronchial biopsies from smokers and patients with COPD. Eur Respir J 2002;20:556–63.

47. Chung KF. Cytokines in chronic obstructive pulmonary disease. Eur Respir J Suppl 2001;34:50–9s.

48. Tang X, Liu D, Shishodia S, et al. Nuclear factor-κB (NF-κB) is frequently expressed in lung cancer and preneoplastic lesions. Cancer 2006;107:2637–46.

49. Huang J, Chen K, Gong W, Dunlop NM, Wang JM. G-protein coupled chemoattractant receptors and cancer. Front Biosci 2008;13: 3352–63.

50. Fraser CC. G protein-coupled receptor connectivity to NF-κB in inflammation and cancer. Int Rev Immunol 2008;27:320–50.

51. Gao H, Sun Y, Wu Y, et al. Identification of β-arrestin2 as a G protein-coupled receptor-stimulated regulator of NF-κB pathways. Mol Cell 2004;14:303–17.

52. Aouadi M, Tesz GJ, Nicoloro SM, et al. Orally delivered siRNA targeting macrophage Map4k4 suppresses systemic inflammation. Nature 2009;458:1180–4.

53. Sarkar FH, Li Y. NF-κB: a potential target for cancer chemoprevention and therapy. Front Biosci 2008;13:2950–9.

54. Li YT, He B, Wang YZ, Wang J. Effects of intratracheal administration of nuclear factor-κB decoy oligodeoxynucleotides on long-term cigarette smoke-induced lung inflammation and pathology in mice. Respir Res 2009;10:79.

Cancer Prevention Research

Knockout of the Tumor Suppressor Gene *Gprc5a* in Mice Leads to NF- κB Activation in Airway Epithelium and Promotes Lung Inflammation and Tumorigenesis

Jiong Deng, Junya Fujimoto, Xiao-Feng Ye, et al.

Updated version	Access the most recent version of this article at: doi:10.1158/1940-6207.CAPR-10-0032
Supplementary Material	Access the most recent supplemental material at: http://cancerpreventionresearch.aacrjournals.org/content/suppl/2010/04/05/1940-6207.CAPR-10-0032.DC1

Cited articles	This article cites 54 articles, 17 of which you can access for free at: http://cancerpreventionresearch.aacrjournals.org/content/3/4/424.full#ref-list-1
Citing articles	This article has been cited by 6 HighWire-hosted articles. Access the articles at: http://cancerpreventionresearch.aacrjournals.org/content/3/4/424.full#related-urls

E-mail alerts	Sign up to receive free email-alerts related to this article or journal.
Reprints and Subscriptions	To order reprints of this article or to subscribe to the journal, contact the AACR Publications Department at pubs@aacr.org.
Permissions	To request permission to re-use all or part of this article, use this link http://cancerpreventionresearch.aacrjournals.org/content/3/4/424. Click on "Request Permissions" which will take you to the Copyright Clearance Center's (CCC) Rightslink site.